THE JOURNAL OF PHYSICAL CHEMISTRY B

Article

pubs.acs.org/JPCB

Parallel Optimization of a Reactive Force Field for Polycondensation of Alkoxysilanes

Joshua D. Deetz* and Roland Faller*

Department of Chemical Engineering & Materials Science, University of California, Davis 95616, California, United States

Supporting Information

ABSTRACT: We have optimized a reactive force field (ReaxFF) in order to model the gelation of alkoxysilanes in bulk precursor solutions. The force field parameter set was refined using a parallelized local search algorithm. Using this approach, each processor is assigned a small list of parameters. At the end of every iteration, all parameters are updated simultaneously after being independently evaluated. In comparison to the serial evaluation of parameters, this results in faster parametrization of ReaxFF, as well as helps to prevent entrapment in local minima. The resulting model is found to reproduce hydrolysis and condensation reaction energies well. By applying the model to the condensation of silicic acid monomers at several temperatures, the activation energy of silane condensation is determined. The expected behavior, a gradual depletion of hydrolyzed silicon and growth of condensed silica clusters is observed over timescales of a few nanoseconds. The new model is also verified by modeling the early stages of clusterization in an alkoxysilane precursor solution. Both hydrolysis and condensation reactions are observed in a system containing a mixture of tetramethoxysilane, methanol, and water.

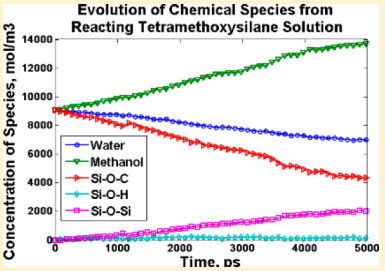

I. INTRODUCTION

Alkoxysilanes have attracted much interest due to their versatile applications, such as coupling agents between metal oxides and polymers,[1] coatings for tribological,[2] organofunctional,[3,4] and corrosion-resistant surfaces,[5,6] as well as bioactive materials,[7] porous gels, and dense solids. The wide variety of technological applications of alkoxysilanes is due to their ability to hydrolyze from individual precursor molecules and subsequently undergo polycondensation[8] to form a wide range of products,[9] such as gels, polymers, and dense solids. Additionally, such reactions can be used to bind chemical groups (e.g., organotrialkoxysilanes)[3] to the surfaces of metal oxides. The hydrolysis and condensation reactions are illustrated in Scheme 1.

The chemistry of sol−gel condensation can be customized to tailor solids and surfaces with desired chemical properties. The morphology of the final product depends on the chemistry of the precursor solution and the reaction conditions. The chemical structure of the precursor alkoxysilane has been shown to affect the kinetics of hydrolysis and condensation,[10−12] manifested through the steric accessibility and polarity of the reacting Si−O bonds. For trialkoxysilanes, the range of products formed is strongly dependent on the headgroup attached to the precursor.[9,13] The solvents used during reaction influence the solubility of the precursor silane.[12,14] Reaction conditions, such as temperature[14,15] and pH,[11] dictate the reaction rates of hydrolysis and condensation.

Due to the large number of process variables which determine the behavior of gelation, it is difficult to control precisely the products and their properties. It would be beneficial to understand how each variable influences the morphology of the products on a molecular level in order to design new materials and processes. Using molecular dynamics, alkoxysilanes have been studied using nonreactive models for different "snapshots" along the gelation process,[16,17] as well as to study their orientation at metal oxide surfaces.[18,19] However, nonreactive models cannot study reacting systems, as they do not break and form chemical bonds. Quantum chemical studies have elucidated the hydrolysis and condensation reaction mechanisms,[20−22] the surface attachment chemistry of alkoxysilanes with silica,[22] and the energetics of different condensed cluster morphologies.[23,24] Empirical models[25−30] have been used to study the polycondensation of tetrahydroxysilane at different reaction conditions, but these have not been expanded to include hydrolysis reactions of alkoxysilanes or the effects of solvents and pH on the final products.

Modeling the hydrolysis and condensation of silanes in solution will provide valuable insight into the underlying dynamics of gel formation. The effects of different reaction conditions could be understood at the molecular level. Elucidating relationships between the reaction chemistry and the final product morphology will benefit the fundamental understanding of gelation. However, a molecular dynamics force field which can model sol−gel reactions of alkoxysilanes does not currently exist.

Due to computational cost, quantum chemical simulations are currently limited to around 1000 atoms.[31] Depending on the reaction conditions and precursor used, the activation energies for the hydrolysis and condensation of alkoxysilanes are reported to be in the range of 5−15 kcal/mol.[14,15,20,21] Due to the relatively high barriers to reaction and limitations on the

Received: April 28, 2014
Revised: August 17, 2014

   dx.doi.org/10.1021/jp504138r | J. Phys. Chem. B XXXX, XXX, XXX−XXX

Scheme 1. Chemical Equations for the Hydrolysis, Condensation, And Alcohol Condensation Reactions of Alkoxysilanes

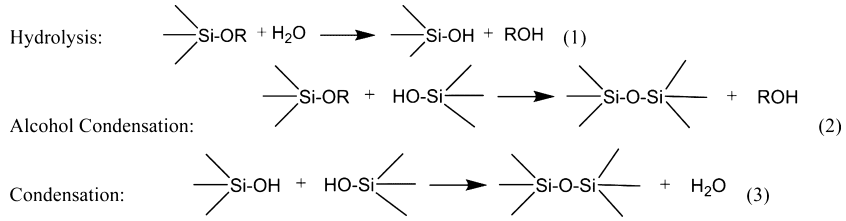

number of basis functions that can be included, alkoxysilane gelation is currently outside the realm of ab initio calculations.

In recent years, an empirical force field, ReaxFF,[32,33] has been applied to model a wide range of reacting systems. This force field allows for chemical bonds to smoothly form and break during simulations. ReaxFF has been parametrized to correctly predict activation energies and heats of reaction.[34] Therefore, it should be able to reproduce the underlying thermodynamics of alkoxysilane condensation. Parameterizations of ReaxFF exist for other silicon-based materials, such as silica (bulk[35] and surface[36]), silicon carbide,[37] and polydimethylsiloxane[38] (PDMS). However, these parametrizations are not optimized for the gelation of alkoxysilanes from precursor solution.

In order for ReaxFF to reproduce chemical reactions, molecular structure, and bulk phase properties, a large amount of data must be used during force field parametrization as ReaxFF contains hundreds of parameters. This can set practical limitations on classes of chemical data that are included in the optimization. Potentially useful properties, such as liquid densities, free energies of solvation, and diffusion coefficients are intractable to optimize against during the force field development process, as they simply take too much computer time to evaluate.

In the majority of ReaxFF parametrizations,[33−35] a single parameter search algorithm[39] is used, which employs a parabolic extrapolation procedure to optimize the force field one parameter at a time. This algorithm is essentially a single processor steepest descents procedure. By parallelizing this optimization procedure, the time required to parametrize a new force field can be substantially reduced and can lead to more fine-tuned models. In this study, we develop a force field for the polycondensation of alkoxysilanes using a parallel local search algorithm. The work of optimizing the force field is divided across several processors which are assigned small lists of parameters. Due to this difference, faster parametrization times can be achieved.

Recently, genetic,[40−42] hybrid genetic conjugate-gradient minimization,[43] and simulated annealing[44] algorithms have been used to optimize ReaxFF force fields. These algorithms all have the advantageous feature of sometimes accepting "bad" solutions, which enhances the exploration of the parameter space and prevents entrapment in local minima. Up until this time, genetic algorithms have only been applied to small subsets of the total parameter space in order to make optimization more feasible. As the number of dimensions in the total searching space increases exponentially with the number of parameters being optimized, it is necessary to restrict their number in order to make global optimization tractable. However, for the end user it is difficult to determine *a priori* which parameters will have the most significant effect on the optimization. The present study does not attempt to perform a fully global optimization or to determine which parameters are the most influential but instead focuses on optimizing a large set of parameters thought to be relevant that are chosen through chemical intuition.

II. METHODS

In this section, we cover the details on the newly developed parallel optimization routine which is used for obtaining the force field parameters and the algorithms implementation. We also discuss the methodology used in the collection of target data, against which the force field is optimized.

Optimization Algorithm. ReaxFF is rooted in the concept of bond order,[45] which is defined as the number of chemical bonds between pairs of atoms. In ReaxFF, the bond order is a continuous function and smoothly turns on and off various potential energy contributions including bond, angle, and dihedral energies. As the bond order approaches zero, these bonded forces are gradually switched off. Therefore, the equations of ReaxFF are highly coupled and subsets of parameters cannot be independently optimized. A typical force field includes hundreds of parameters, making it difficult to discriminate which parameters are the most important to optimize.

The parametrization of ReaxFF fits the parameter set to a collection of data describing the system, which is referred to as the training set. The training set is comprised of such information as partial atomic charges, molecular geometry, bulk phase data, or energy differences between states. These pieces of information are obtained from both quantum chemical calculations and experimental data.

Each piece of information in the training set is assigned a weight, which attributes its level of importance to the parameter optimization. The differences between the properties defined in the training set and the corresponding values calculated by the parameter set define a set of discrepancies; the sum of their squares is the penalty function, P (eq 1). $V_{i,\mathrm{train}}$ is a property defined in the training set, $V_{i,\mathrm{reax}}$ is the predicted property by the parameters, and ω is the inverse weight on the training set property.

$$P = \sum_{i}^{\text{training set}} \left(\frac{V_{i,\mathrm{train}} - V_{i,\mathrm{reax}}}{\omega^{*} V_{i,\mathrm{train}}} \right)^{2} \quad (1)$$

The penalty function is defined in a space spanned by the N optimization parameters of the force field. Finding the global minimum in this space is the goal of force-field parametrization. It is often necessary to minimize the dimensionality of the parameter space for the optimization to be tractable.

There are obvious advantages to the use of parallel optimization algorithms. The optimization can be more efficient by dividing computations among many processors. In the present study, we have developed a "parallel parameter search" technique. A schematic of this algorithm is shown in Figure 1. The parallel parameter search algorithm divides the list of parameters into multiple smaller lists and assigns these to

dx.doi.org/10.1021/jp504138r | J. Phys. Chem. B XXXX, XXX, XXX−XXX

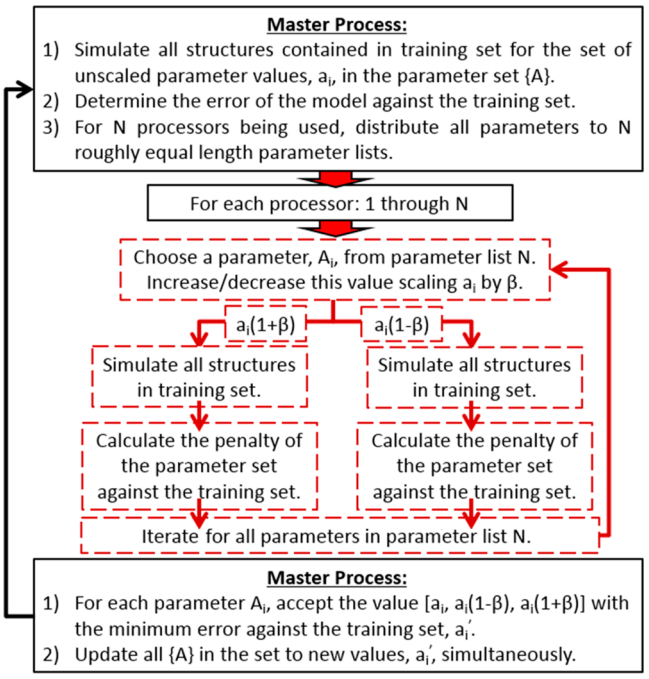

Figure 1. Workflow of parallel optimization routine. At the start of each iteration the parameter list is divided among N processors, with each processor focusing on a smaller list of parameters. The unscaled parameter values, a_i, are only evaluated once. Next, all of the scaled parameters, $a_i(1 + \beta)$ and $a_i(1 - \beta)$, are evaluated on their respective processors. At the end of the iteration, all parameters are updated simultaneously, changing to the value that minimizes the penalty function against the training set.

each node. For a given parameter, A_i with a value a_i, the penalty function is evaluated by simulation at values of $A_i = a_i$, $A_i = a_i(1 + \beta)$, and $A_i = a_i(1 - \beta)$ and the value which minimizes P is selected, where β is the scaling factor. All parameters $\{A\}$ are updated simultaneously at the end of each iteration.

There are a few distinctions between the parallel parameter search algorithm and the single parameter search technique,[39] on which this algorithm is based. The single parameter search method uses four evaluations of the training set per parameter. Using this method to evaluate one parameter, A_i, with scaling factor β, the candidate values of $A_i = a_i$, $A_i = a_i(1 + \beta)$, and $A_i = a_i(1 - \beta)$ are evaluated. Each of these values for parameter A_i will yield a value for P. By fitting a parabola to these three points, a fourth candidate value $A_i = a_i^*$ can be determined at the minimum of this parabola. The parallel parameter search algorithm does not use the extrapolation step. One additional difference between the single and parallel parameter search algorithms is how the parameters are updated. Single parameter search updates the parameter list sequentially after each individual parameter has been evaluated. Using the parallel parameter search technique, all parameters are updated simultaneously at the end of evaluating the entire set. Using this approach, the parameter list does not change before the update step. Thus, the unscaled parameter set $A_i = a_i$ only needs to be evaluated once at the beginning of each iteration and can be used for the whole set $\{A\}$. In our parallelization, only the two new candidates, $a_i(1 + \beta)$ and $a_i(1 - \beta)$, are evaluated for each parameter. This approach could be interpreted as a parallel greedy algorithm,[46] where local changes are made in hopes of finding the optimal solution.

Compared to the single parameter search technique, smaller scaling factors β are used to prevent instabilities which can occur as a result of the simultaneous update. This is especially true with EEM[47] parameters for the atomic charges. In practice, it is desirable to use as large a scaling factor as possible. With the use of a high initial scaling factor, the exploration of the parameter space is promoted, reducing the likelihood of the optimization becoming stuck in a local minimum. In the final stages of the optimization, the scaling factor is gradually reduced to fine-tune the parameters.

For the optimization, we use a serial version of LAMMPS,[48,49] a molecular dynamics code developed by Sandia National Laboratories, in conjunction with a set of Octave[50] scripts which are used to execute simulations and analyze the output. During each iteration, changes are made to the parameter set and each structure in the training set is evaluated using LAMMPS. The output from each of these evaluations allows the penalty function to be computed from eq 1. The programs used for optimization are included as part of the Supporting Information.

Force Field Optimization. In the present study, quantum chemical calculations were used to obtain local structures and energies as part of the training set. Gaussian03[51] was used to perform these QC calculations. In all cases, at least DFT-B3LYP[52,53]/6-311G(d,p)[54,55] level of theory was used to obtain all reaction, energetic, and molecular geometry data. The information collected in the training set is summarized in Table 1.

The atomic coordinates for reaction structures were obtained from Okumoto, Fujita, and Yamabe.[20] This study includes hydrolysis and condensation reaction data for alkoxysilanes reacting with water clusters of various sizes. Reaction structures for the alcohol condensation reaction (the direct condensation of alkoxysilane and silanol to produce alcohol) were added to this set by replacing the leaving hydroxyl group in the condensation reaction (reaction 3) with an alkoxy group. All reaction structures, including the reactant and product complexes as well as transition states, were optimized using the Schlegel algorithm.[56] The transition states of each reaction type were verified by ensuring only one imaginary frequency of

Table 1. Summary of Training Set Used in Optimization

information source	information gathered	examples
optimized molecular structures	atomic point charges, bond lengths, and valence angles	optimized structure of reactant and product states
distortion energy scans	energy differences resulting from changing atomic coordinates along a dimension	bond dissociations between X−Y, angle energy scans between X−Y−Z, and hydrogen and van der Waals bond dissociation
reaction path structures	energy differences along reaction pathway, additional charges, bond lengths, and angles	atomic coordinates of frames along reaction paths for hydrolysis and condensation
crystal structures obtained from X-ray diffraction	crystal lattice parameters (a/b/c/α/β/γ)	lattice parameters of α-cristobalite, ice-1h, etc.

dx.doi.org/10.1021/jp504138r | J. Phys. Chem. B XXXX, XXX, XXX−XXX

Table 2. ReaxFF Parameters Included in Optimization

parameter class	which parameters are optimized	reason for inclusion
general	over/undercoordination parameters	stability of the transition states are affected by over- and under-coordination energy penalties
valence bond	bond order, radii, and bond dissociation energy parameters for O−Si, O−H, H−Si, and C−Si	model reaction pathway and the energetics of bond formation/breakage accurately
valence angle	all parameters for Si−O−H, O−Si−O, Si−O−Si, H−O−H, O−H−O, Si−O−C, H−Si−O, and C−Si−O angles	energetics of valence angles need to model accurately the evolution from reactant states to hyper-valence transition states
van der Waals	van der Waals radii, dissociation energy, and nucleus screening parameters for all combinations of atom types	predict chemical bonding and phase behavior accurately
electrostatic	electronegativity equalization method (EEM) parameters for C, H, O, and Si	predict chemical bonding and phase behavior accurately
hydrogen bond	all parameters for O−HO hydrogen bond	hydrogen-bonded complexes will determine the local environment near reaction centers

vibration. The IRC[57,58] (intrinsic reaction coordinate) module of G03 was used to obtain 48 points (24 in the forward direction and 24 in the reverse direction) along each reaction path in the vicinity of the transition state. Additional points on each reaction path were obtained by energy minimizing the first and last points along this path all the way to the reactant and product states, ensuring a complete sampling of the reaction path. During force field optimization, each frame along the reaction path is energy-minimized. In order to prevent each frame on the reaction path from minimizing to the products or reactants, the reacting bonds are restrained using a harmonic potential. With the use of this method, each point along the path relaxes as closely as possible with the ReaxFF reaction path.

Molecular geometry information, such as bond lengths and valence angles, was also added to the optimization for several alkoxysilanes, such as methyltrimethoxysilane and triethoxysilane, from density functional theory calculations. The geometry of hydrogen-bonded molecular clusters, including several combinations of water, alcohols, and alkoxysilanes, were included as well. The dissociation energy of hydrogen bonding was determined by performing an energy scan on the separation of two water molecules. The geometry of hydronium clusters, such as $H_5O_2^+$ and $H_9O_4^+$, were included in the optimization by obtaining their structure using MP2[59]/6-311G ++(d,p). All optimized molecular structures were included with all bond lengths and angles between bonded atoms. The atomic point charges were added for each molecular structure in the training set. Charges were computed by using a grid-based electrostatic potential solver, CHELPG.[60] Various energy scans were included in the training set. Energy scans are defined as the energy differences resulting from a series of geometric distortions, such as capturing a series of frames along a bond dissociation. Energy scans along the compression and lengthening of the Si−O and O−H bonds were performed, paying special attention to the singlet-to-triplet electronic transition. Several angle energy scans were included in the optimization, such as the Si−O−H and O−Si−O angles. A hydrogen transfer energy scan between H_3O^+ and H_2O was added.

To capture phase information, two kinds of information were added to the training set: crystal lattice parameters and energy scans of dissociating van der Waals clusters. Crystal structures obtained from X-ray diffraction data, including α-cristobalite,[61] solid ethanol,[62] and ice Ih[63] are all included in the optimization. Energy scans of dissociating several small molecular clusters, which are combinations of methane, silane, and water molecules, were added at the level of theory of MP2[59]/6-311G++ (3pd,3df). These two classes of data were included in the optimization because they are useful proxies for long-range forces.

In order to optimize the force field, 192 parameters were selected to comprise the parameter set. Table 2 contains a summary of the classes of parameters. Any parameters relating to the O−H and O−Si bonds were selected as they are essential to the dissociation and formation of bonds during hydrolysis and condensation reactions. Similarly, parameters which represent the over- and under-coordination of Si, O, or H were included as they determine the stability of the transition state. Essential angle parameters relating to Si−O−H, O−Si−O, Si−O−Si, H−O−H, O−H−O, and Si−O−C were all selected as for both hydrolysis and condensation, the transition state has silicon in a penta-coordinate complex.[20] Thus, the force field needs to be able to smoothly transition into and out of hyper-valence states for silicon and oxygen. Hydrogen bonding parameters were added for O−H−O hydrogen bonds, as these structures will be important to determine the stability of the transition state, as well as the path taken by the hydrolysis and condensation reactions.[20] All van der Waals and EEM[47] parameters are also incorporated for the purpose of incorporating bulk phase data into the model.

The parameter values chosen to initialize the optimization are from the ReaxFF set optimized for the corrosion of silicon carbide.[37] This particular parameter set was chosen over others,[36,38] due to our observation that the liquid densities of water, alcohols, and precursors more closely matched expectations. In principle it is possible to choose any parameter set containing the relevant atoms as a starting point for the optimization, but in practice it is best to test several sets of parameters and to start from the force field which most closely matches the training set.[43] It was noticed prior to optimization that simulating liquid water using ReaxFF parameters developed for PDMS[38] and SiC corrosion[37] led to several hydrogen atoms being under-coordinated and forming unphysical hydrogen−hydrogen bonds. This effect led to unrealistic liquid densities for water, such as 2.7 g/cm^3 for the PDMS parameter set. It has been reported before that the transferability of ReaxFF parameters is limited.[44] Thus, even if the required atoms are present in a reactive force field for a given application, it is necessary to be cautious and verify the model's accuracy. A similar behavior was observed between methyl hydrogens and water hydrogens. To fix this, we added energy scans of the dissociation of water and methane as well as dissociating two water molecules to the optimization. These energy scans are performed with the hydrogen atoms facing each other and measure energy at different separation distances. As hydrogen atoms participate in all condensation and

dx.doi.org/10.1021/jp504138r | J. Phys. Chem. B XXXX, XXX, XXX−XXX

hydrolysis reactions, it was anticipated that maintaining the chemistry for hydroxyl hydrogens and methyl hydrogens simultaneously would be difficult. Similar in philosophy to other force fields,[64,65] we have adopted a convention in which there are two hydrogen atom types, "H" for hydrogen atoms attached to oxygen atoms, and "Hc" for hydrogens bonded to either silicon or carbon. It is not anticipated that these two atom types will ever switch places as all methyl hydrogens are attached to their respective molecules by restraints such that their bonds never break.

The 192 parameters selected for optimization are distributed among 64 processors. Any number of parameters or processors can be used, and the implementation of the algorithm is not restricted to evaluating a limited number of parameters. The weights on all pieces of information in the training set were assigned by first calculating the penalty function of the unoptimized model P_0. The weights on all atomic charges in the training set were assigned such that their contribution to the penalty function combined to 1/6 P_0. Similarly, energy scans were also assigned 1/6 P_0. Molecular geometry information and bond lengths and angles, including the geometry of each transition state, were assigned $1/3P_0$. Reaction path energies and crystal structures were assigned the remainder of P_0.

We optimize the parameters initially using a scaling factor of β = 0.05 for most parameters, using half this value for any global or atom-specific parameters, as these are more sensitive to changes. After every four iterations, we geometrically decrease the scaling factor by 10% of its current value to progressively focus on fine-tuning the parameters.

The optimization is stopped after any changes to the parameter set, using a scaling factor β = 0.005, no longer reduce P. For scaling factors below this, it is typically found that there is not any significant improvement in the model, and only random fluctuations within 5% of the penalty occur. This was achieved after 48 iterations of parameter changes. After this initial phase, subsequent optimization was used in which the weights on the reaction path energies were increased (making them a more important contribution to the penalty function) in order to ensure that the optimized parameters predict reaction energies accurately. This phase used 88 iterations to further optimize the model.

The implementation of the parallel parameter search algorithm was performed on a Red Hat cluster using 8 nodes in which each node has eight Intel Xeon E5620 CPUs with 8GB of memory. For comparison purposes, we have also implemented the single parameter search algorithm on Ubuntu 12.04 using an Intel i7 3537U CPU and 8GB of memory.

III. RESULTS

IIIa. Parallel Optimization Algorithm Performance. Figure 1 depicts a detailed workflow diagram of the parallel optimization approach in this study. The optimization space spans 192 parameters on 64 processors, which were chosen using the methodology described above. It is found that each iteration, a single pass through the entire parameter set, can be completed in 25−40 min using an Intel Xeon E5620 CPU with 8 GB of memory. In our implementation of the single parameter search (SPS) algorithm, each iteration took between 12 and 14 h using an Intel i7 3537U CPU and 8 GB of memory. However, when SPS is compared side-by-side with the parallel parameter search algorithm on the same hardware, 31 h were required to complete one iteration. Thus, depending on the system hardware being implemented, a potential speed boost of 18 to 74 fold can be obtained from using the parallel parameter search technique.

With SPS, the parameter set is updated sequentially after evaluating each parameter. For each parameter in the list, small local changes are tested and only accepted if they lower P. Thus, the penalty function decreases monotonically. This approach is prone to becoming stuck in local minima. The only way SPS can escape local minima is if the changes which are evaluated for a particular parameter are high enough that they can "see" a neighboring minima which is even lower than the current state.

The parallel parameter search algorithm updates all parameters simultaneously at the end of each pass-through the parameter list. Sometimes, performing multiple changes to the parameter set simultaneously can have the effect of increasing the penalty function, due to the intercorrelated nature of ReaxFF equations. However, this increase can sometimes have a beneficial side effect of promoting some additional exploration of the parameter space before settling down in a minimum.

Figure 2 illustrates these points. The SPS algorithm and the parallel optimization routine are compared by optimizing the same parameter list and using the following sample procedure, which is different from the procedure used to optimize the model. For the parallel optimization, the first four parameter updates use a scaling factor of β = 0.05. After these iterations, the scaling factor is lowered by 30% every four iterations until β = 0.005 is reached, at which point optimization ends. The SPS optimization in Figure 2 follows a similar procedure, except that a period of two iterations is used between adjusting the scaling factor, instead of four. As can be seen in Figure 2, the convergence of the parallel algorithm is faster than SPS. The

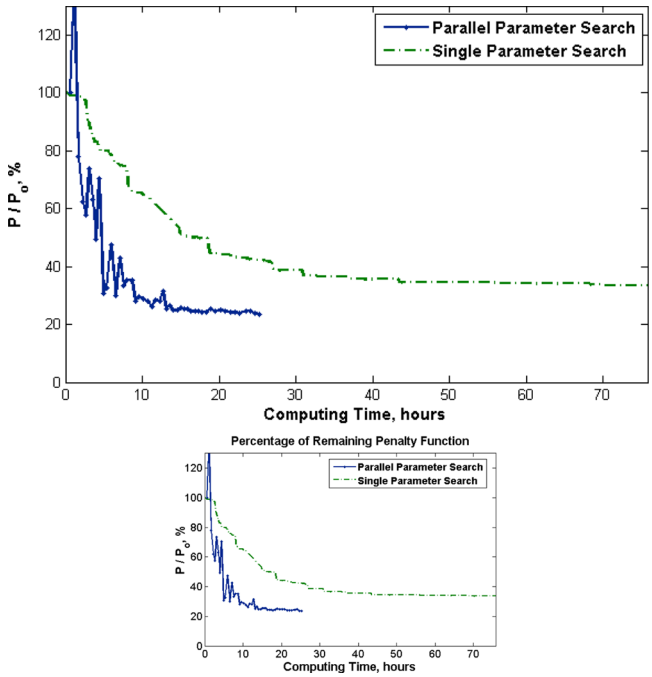

Figure 2. Comparison of performance of single and parallel parameter search algorithms. The y-axis shows the current penalty function expressed as a percentage of the initial penalty function prior to optimization.

dx.doi.org/10.1021/jp504138r | J. Phys. Chem. B XXXX, XXX, XXX−XXX

parallel optimization algorithm in this example also reaches a lower minimum than SPS, as the simultaneous parameter update enables more exploration of the parameter space.

As seen in Figure 2, initially the SPS converges to the training set quickly. However, the optimization soon becomes stuck in a local minimum from which it cannot escape. Previous studies have also shown SPS to converge to local minima.[40,44] Aside from being inherently a local minimum search algorithm, this is also because SPS focuses on adjusting single parameters sequentially. In the initial stages of the optimization, it is easier to find an adjustment to the parameters in order to decrease the penalty function. Because the parameters are evaluated sequentially down a list, the order of the parameters in this list affects the outcome of the optimization, with parameters situated earlier in the list more likely to change than those evaluated later. The parallel optimization algorithm solves this issue by evaluating all parameters simultaneously, rather than in a sequential list.

Among the 192 parameters chosen for optimization, SPS converges to a local minimum after an average 1.2% change to the initial values of the parameters, with standard deviation of 2.1% and a maximum of 14.8% change to a single parameter. After convergence of the parallel parameter search algorithm, there is an average of 7.9% change to the parameters, with a standard deviation of 8.1% and a maximum of 51.4%. It is clear that even though the two algorithms begin from the same parameter set, they converge to entirely different minima. It is also evident that even though only small changes were made to the parameter set (at an average of eight percent), the penalty function has substantially decreased. This is due to the fact that the majority of parameters in ReaxFF are exponential factors, which are highly sensitive to even small changes. Another metric of performance is the number of parameters which are left unchanged by each algorithm. After convergence, SPS leaves unchanged 78 of the 192 parameters, whereas the parallel parameter search has changed all but 8. This implies that the parallel parameter search is more robust in the exploration of the parameter space, even if the exploration is only local.

Recently, genetic algorithms[40−43] have been investigated in optimizing ReaxFF parameter sets. While genetic algorithms are promising to enable global exploration of the error space, so far all of the implementations focus on a smaller subset of the total parameter set. For instance, sets of 37,[43] 51,[40] and 67[41,42] parameters in the set are chosen for optimization in these implementations. The decision to focus on a small subset of parameters was necessary to make optimization feasible by restricting the size of the searching space. The size of the optimization space increases exponentially with the number of parameters being changed. Due to the computational expense of evaluating the training set during each iteration, it is necessary to limit the number of parameters being optimized. Unfortunately, it is not always clear which parameters will be the most significant in optimizing toward the training set data, and it becomes necessary to determine this in a systematic way. Pahari and Chaturvedi[40] used a genetic algorithm to optimize a C/H/N/O parameter set. They initially started with a full set of 611 parameters. By first determining which parameters had a significant impact on the penalty function (above a certain threshold), and subsequently measuring cross-correlations between each parameter and the training set properties, the parameter set was reduced to 51 significant parameters. Recently, a genetic-algorithm-based framework for optimizing reactive force fields,[43] GARFfield, has been developed. At the present, there does not appear to be a systematic way to find significant parameters, and such an implementation would be extremely useful.

Regardless, global and local optimizations should be used together to first find the vicinity of the global minimum and subsequently converge to lowest value of the penalty function. In the present study, it was not necessary to reduce the size of the parameter set through any sort of screening procedure because global exploration was not attempted. The choice of a good starting point for the optimization facilitated the convergence to good agreement with the training set properties. All parameters believed to be relevant to the chemical system being studied are optimized, which are selected on the basis of chemical intuition.

IIIb. Force Field Optimization for Alkoxysilanes. After the parallel optimization had converged using the procedure described at the end of Methods, the resulting properties of the force field were validated for consistency with the training set. Figures 3 and 4 show the bond dissociation energies for C−Si and O−Si bonds, respectively. The ab initio energy is taken to be the minimum energy calculated between the singlet and triplet electronic states for each point. The bond dissociation energy has converged in both cases to the data collected from density functional calculations. However, the shape of the energy wells is not an exact match, which could influence the frequency of bond vibrations. The dissociation energy curves for other pairs of atoms are also in good agreement. The dissociation energy for O−H bonds in water is calculated to be 138 kcal/mol, whereas the ab initio value is 118 kcal/mol. Additionally, the length of the O−H bond is about 0.90 Å, as opposed to typical values of 0.96−0.98 Å from our quantum chemical calculations. This difference is attributed to the curvature of the energy well in the O−H bond, which is an important factor for the curvature of the reaction pathway for

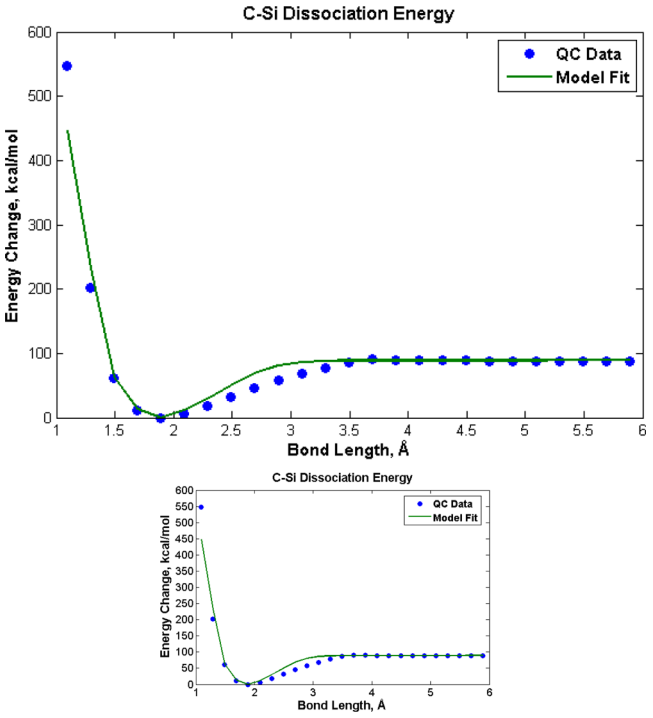

Figure 3. Bond dissociation energy of C−Si bond in methyltrimethoxysilane.

dx.doi.org/10.1021/jp504138r | J. Phys. Chem. B XXXX, XXX, XXX−XXX

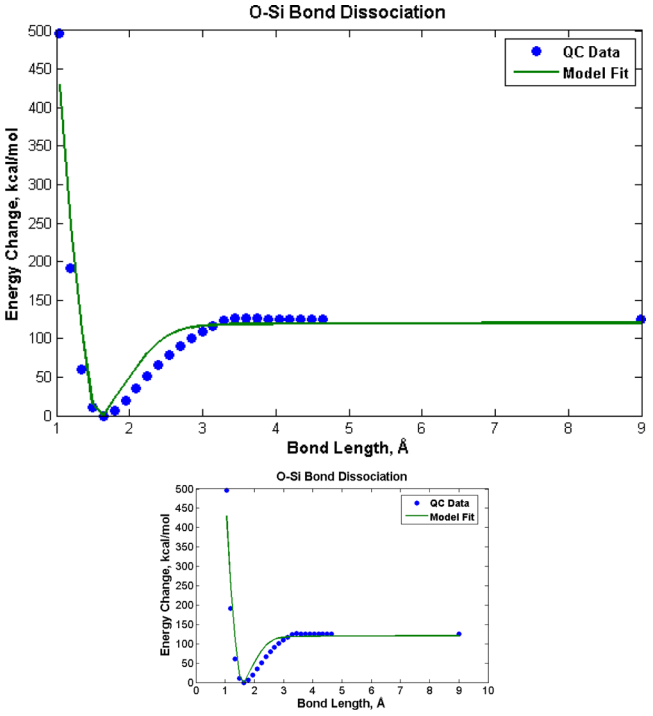

Figure 4. Bond dissociation energy of O−Si bond in trihydroxysilane.

hydrolysis and condensation. As higher weights have been assigned to the reaction energies as opposed to the bond dissociations, the optimization models the reaction pathways more accurately. These differences are not expected to be important, as only in extreme situations is bond dissociation is expected.

In order to investigate typical atomic partial charges predicted by the model, a representative molecule methyl-dihydroxy-methoxy-silane is chosen (MDHMS). This chemical species is unstable in solution but is used here for purposes of illustration. The atomic map of this molecule is shown in Figure 5. Table 3 shows the convergence of atomic point charges of

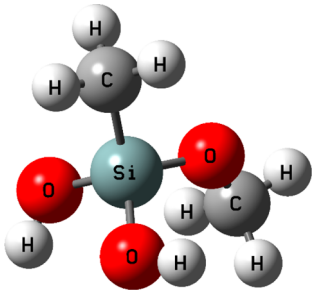

Figure 5. Elemental map of methyldihydroxymethoxysilane (MDHMS).

MDHMS computed by EEM[47] to charges determined by density functional theory using CHELPG.[60] The atomic charges on the essential reacting atoms in this structure (Si, O, and H) are all consistent. If a hydrogen atom is used as a headgroup to the central silicon atom, such as that of trimethoxysilane, the correct trend of assigning a negative charge to hydrogen is observed, as hydrogen is more electronegative than silicon.

Table 3. Comparison of Atomic Point Charges for MDHMS (shown in Figure 5) Determined Using Optimized Model and Ab Initio Calculations

atom	description	QC charge (CHELPG)	fitted model
Si	central Si atom	1.151	1.094
O	alkoxysilane O atom	−0.560	−0.545
O	hydroxyl O atom	−0.741	−0.723
C	headgroup C atom	−0.628	−0.446
C	alkoxysilane C atom	0.208	0.062
H	hydroxyl H atom	0.426	0.414
H	methyl H atom	0.076	0.076

Table 4 shows typical bond lengths resulting from the geometry optimization of molecular structures in the training

Table 4. Comparison of Typical Bond Lengths in Optimized Model Versus Ab Initio

	bond length (Å)	
bonds	fitted model	QC
O−Si	1.64	1.66
C−Si	1.91	1.86
H−Si	1.48	1.48
O−C	1.44	1.43
O−H	0.92	0.96
C−H	1.09	1.10
C−C	1.54	1.52

set. In most cases, chemical bond lengths in the model are close to the value determined by density functional calculations. The bond between oxygen and hydrogen atoms is predicted to be shorter and stiffer, but this is ascribed to the additional accuracy desired in predicting the correct activation energies.

All reaction transition structures used for optimization were obtained from the density functional theory calculations[20] of Okumoto et al., which studied the gas phase reactions of alkoxysilanes with water clusters of various sizes. For all reactions in Scheme 1, Table 5 shows the predicted activation

Table 5. Predicted Reaction Energies for Hydrolysis and Condensation of MDHMS (Shown in Figure 5)

	activation energy		energy of reaction	
reaction	DFT	model	DFT	model
hydrolysis	24.38	27.0	−6.45	−9.41
condensation	28.46	29.2	−3.69	−4.96
alcohol condensation	26.69	27.6	−7.42	−6.93

and heat of reaction energies for the optimized model. For each reaction, the activation energy is the difference between the energy of the transition state (the highest energy on the reaction path) and the reactant complex (the minimum energy structure of the reactants together). The heat of reaction is the energy difference between the reactant and product complexes. In Table 5, all reaction energies are predicted well. The energy released by hydrolysis is slightly too exothermic. These energies are determined for gas-phase reactions, but liquid phase reactions are more important. Typically, the liquid phase activation energies of sol−gel reactions of alkoxysilanes are in the range of 5−15 kcal/mol,[14] depending on the reactants and conditions used. The difference between the liquid and gas phase activation energies can be attributed to the stabilization

dx.doi.org/10.1021/jp504138r | J. Phys. Chem. B XXXX, XXX, XXX−XXX

Table 6. Predicted Lattice Parameters of Several Crystals

description	lattice parameters (a/b/c/α/β/γ) experimental (Å/Å/Å/deg/deg/deg)	lattice parameters (a/b/c/α/β/γ) model[a] (Å/Å/Å/deg/deg/deg)	% error density	COD ID no.[b]
tetraisopropoxysilane	8.04/8.04/24.65/90/90/90	8.21/8.19/25.50/90/90/90	7.6	4116968[71]
hydrogen-silsesquioxane	9.05/9.05/15.15/90/90/120	8.96/8.96/15.12/90/90/120	2.2	2010158[72]
α-cristobalite	4.97/4.97/6.92/90/90/90	5.16/5.16/7.13/90/90/90	11.1	9009685[61]
Ice-1h	7.82/7.82/7.36/90/90/120	8.16/8.15/7.58/90/90/119.9	12.1	1011023[63]
solid methanol	4.65/4.93/9.04/90/90/90	4.31/5.24/8.93/90/90/90	2.7	4503066[73]
solid ethanol	5.38/6.88/8.26/90/102.2/90	5.37/6.95/7.84/90/105.4/90	5.6	5910115[62]
trans-1,4-dimethylcyclohexane	6.08/5.48/11.80/90/103.9/90	6.01/5.52/11.76/90/104.9/90	0.9	4116968[74]

[a]Lattice parameters obtained after potential energy minimization for each solid (see section Force Field Optimization for Alkoxysilanes). [b]Crystallography Open Database ID no. (http://www.crystallography.net/).

of transition structures by hydrogen bonding in the vicinity of the reacting bonds. In the next section, this difference in activation energy is directly observed with the condensation of tetrahydroxysilane in solution.

One of the limitations of ReaxFF which differentiates it from nonreactive force fields is how chemical bonds are treated. In nonreactive force fields, the equations for chemical bonds have attractive and repulsive distances depending on if the two-bonded atoms are too compressed or stretched. In the case of ReaxFF, however, a repulsive bond component is not used,[32,33] instead the repulsive van der Waals component is used simultaneously for bonds as well as for long-range forces. This characteristic complicates the optimization of ReaxFF against bulk phase data, such as liquid densities, because any changes to the parameters for long-range forces will also have an effect on the repulsive regime of local bonding. Recently, a new implementation, ReaxFF-lg,[66] has proposed that a dispersion correction function be added to the potential equations of ReaxFF. In theory, this can enhance the capability of ReaxFF to accurately predict both bulk phase properties and local molecular structure and bond energies. In order to test the accuracy of the optimized model, the properties of several solids and liquids are reported in Tables 6 and 7. For solids, the lattice parameters were obtained by performing energy minimization while allowing the simulation box dimensions (a/b/c/α/β/γ) to change. To allow the box to deform, the Parrinello–Rahman barostat was applied to the box at 0 bar during minimization. The liquid systems in Table 7 were simulated by filling a box with dimensions 24 × 24 × 24 Å^3 with the number of molecules required to match experimental density (rounded up). Each system was simulated in the isobaric–isothermal ensemble at 300 K and 1 bar, using the Nosé–Hoover barostat[67,68] with the time constant of 250 fs, and thermostat[69,70] with the time constant of 25 fs. In general, the error in densities predicted by the optimized force field versus experimental data rarely exceeds 10%.

Table 7. Predicted Densities of Several Liquids at STP (298 K, 1 bar)

description	experimental density (g/cm^3)	model density (g/cm^3)	% error
water	0.997[75]	1.088 ± 0.016	8.8
methanol	0.787[75]	0.829 ± 0.039	4.6
tetramethoxysilane	1.023[75]	0.975 ± 0.054	4.7
trimethoxysilane	0.961[76]	0.850 ± 0.083	8.3
methyltrimethoxysilane	0.955[77]	0.888 ± 0.059	5.9

IIIc. Case Study: Pure Silicic Acid Condensation. In order to test the accuracy of our newly optimized model for the polycondensation of alkoxysilanes, we have simulated the condensation of tetrahydroxysilane in the liquid phase. This system has been studied many times previously.[25−29] Following a similar procedure to that of Rao and Gelb,[29] we simulated 729 molecules of tetrahydroxysilane. The size of the simulation box was calculated by assuming a density of 1.0 g/cm^3 in which the molecules were randomly dispersed using Packmol.[78] This system was simulated using LAMMPS[48,49] at a series of temperatures: 1000, 1500, 1750, and 2000 K, using the canonical ensemble. The equations of motion were integrated by using the velocity-Verlet algorithm with time step of 0.25 fs. The temperature was maintained using the Nosé–Hoover thermostat[69,70] with a time-damping constant of 25 fs.

Figure 6 shows the temporal evolution of condensed silicon bridges (Si–O–Si) at different temperatures. Between 1500 and 2000 K, our model predicts a rapid condensation of silicic acid while generating stoichiometric amounts of water and

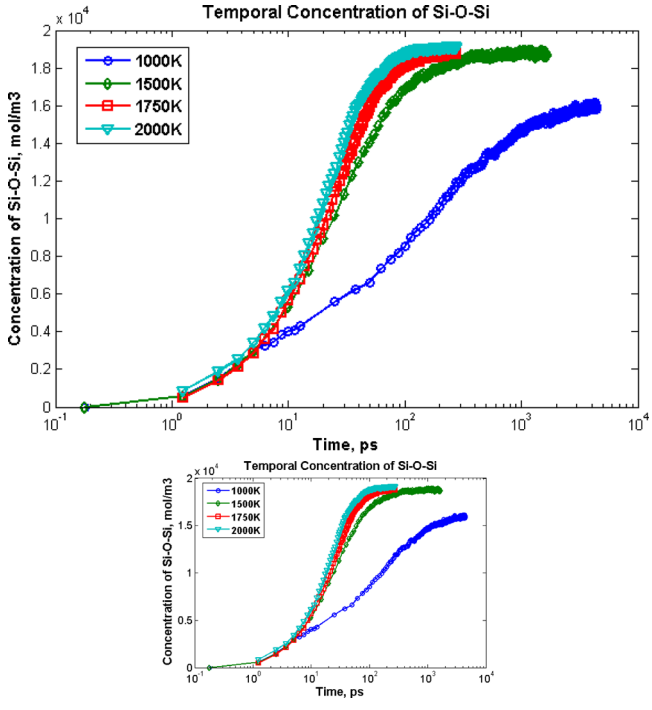

Figure 6. Temporal concentration profile of Si–O–Si for during gelation of pure silicic acid.

dx.doi.org/10.1021/jp504138r | J. Phys. Chem. B XXXX, XXX, XXX–XXX

consuming hydrolyzed silicon. At 1000 K, the kinetics of condensation are significantly slower. As the silanols undergo polycondensation, clusters of siloxanes form. The maximum cluster size is monitored in Figure 7. Between 1500 and 2000

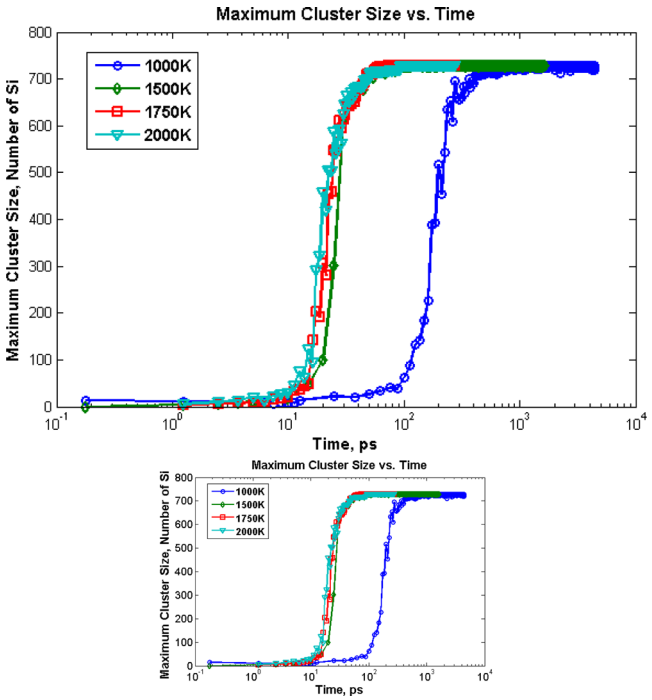

Figure 7. Temporal evolution of maximum cluster size in simulation of pure silicic acid gelation.

K, a rapid clustering is seen until the simulation box is fully depleted of uncondensed silicon. At 1000 K, a slower growth of clusters is observed in which after 300 ps of simulation the majority of silicon is condensed. After this time, most of the silicon is condensed into one large cluster, but nearly half of the silanols in the system are unreacted, implying that the cluster is not fully densified.

Figures 8 and 9 show the number of siloxane bridges each silicon atom participates in versus time. At all temperatures, it can be seen that initially the system is dominated by uncondensed silicon, which progressively gives way to silicons with one bridge, two bridges, and so on. This progressive behavior of silicon bridge saturation has been observed in other molecular dynamics studies.[28,29] After 4.5 ns at 1000 K, the system has not reached equilibrium. At 1500 K, linearly bridged and dimer silicon quickly vanish in favor of silicons bearing three and four bridges. Eventually the simulation stabilizes with silicons that have four bridges being dominant. At 1000 K, after 4.5 ns the dominant modes are silicons with three bridges. At 1000 K, 4.5 ns of simulation time was not enough to see a complete depletion of silanols and full densification has not occurred. The formation of condensed clusters occurs quickly (within 400−500 ps), but these clusters consist mainly of silicons with only 2 or 3 bridges. After this initial period, all silicons in the simulation belong to a single large cluster. The remaining simulation time has a transition from two-bridged silicon to three-bridged silicon. This suggests the possibility of multiple timescales for condensation. The initial phase will involve quick clusterization, whereas longer timescales are required to see full densification of these clusters. This agrees

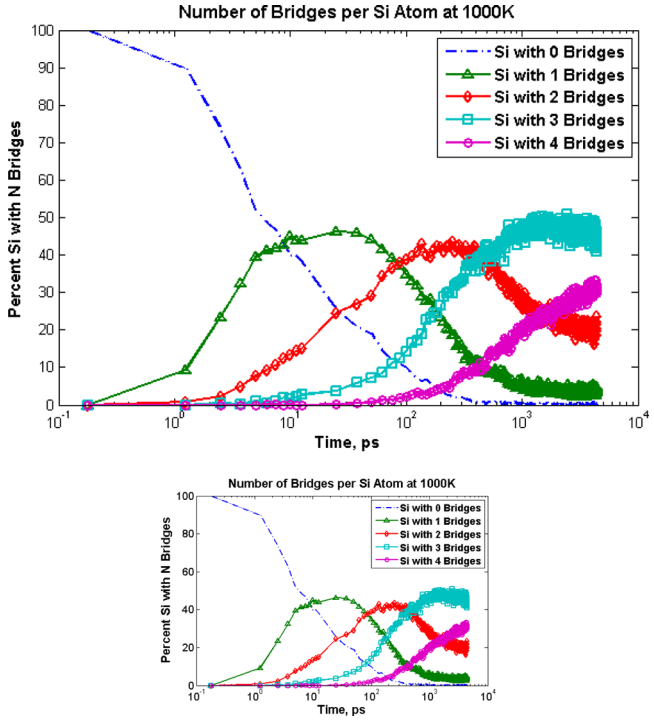

Figure 8. Si bridge distribution for pure silicic acid condensation at 1000 K. The profile depicted here was not simulated to equilibration and is only used to extract dynamic reaction information.

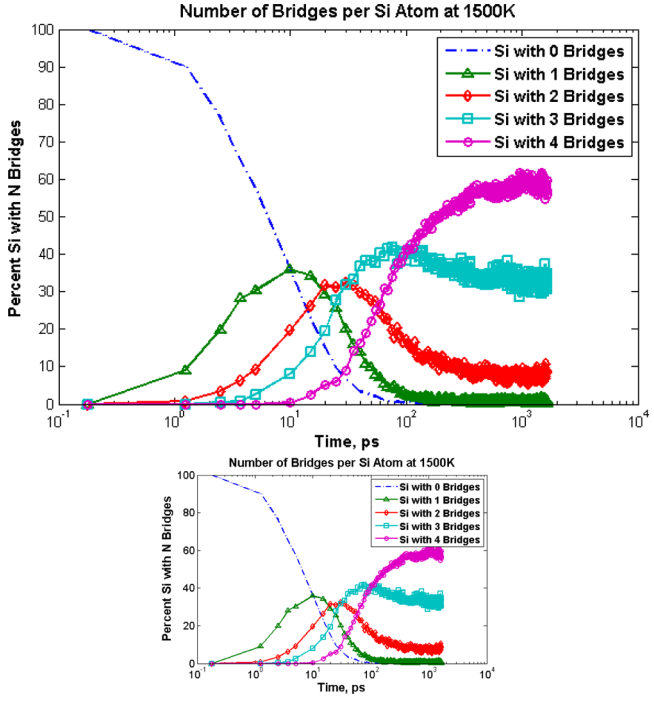

Figure 9. Distribution of Si with different numbers of Si−O−Si bridges for pure silicic acid condensation at 1500K.

well with previous findings that predict multiple timescales for gelation and bulk densification.[30]

The distribution of cluster sizes in the system was also monitored over the course of the simulation. Figures 10 and 11 show the evolution of different size clusters. At 1000 K, smaller cluster sizes have a longer lifetime and abundance than at 1500 K. Additionally, the temporal fluctuations in cluster distribution

dx.doi.org/10.1021/jp504138r | J. Phys. Chem. B XXXX, XXX, XXX−XXX

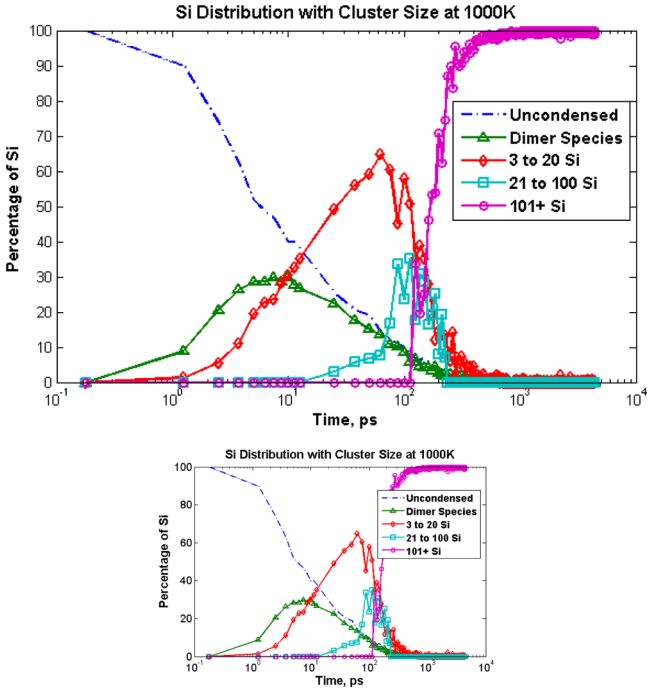

Figure 10. Cluster size distribution at 1000 K in simulation of silicic acid monomers. The profile depicted here was not simulated to equilibration and is only used to extract dynamic reaction information.

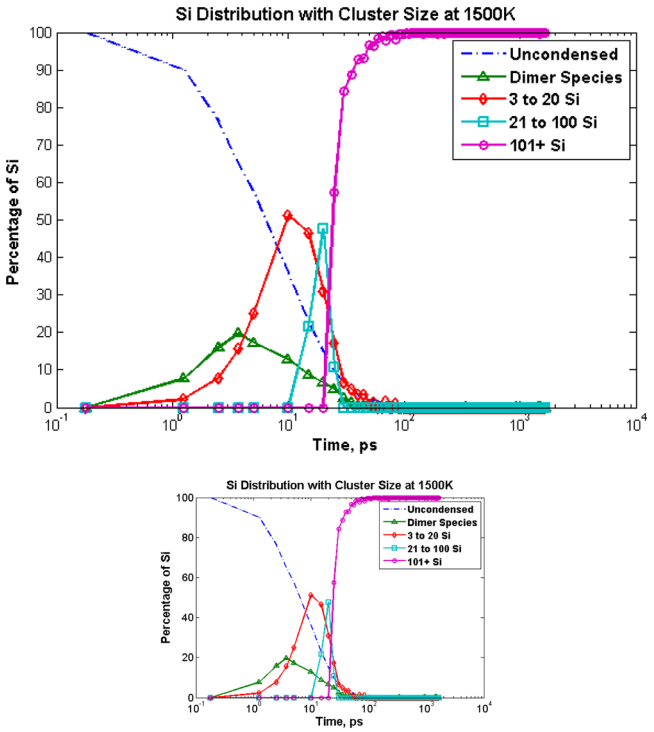

Figure 11. Cluster size distribution at 1500 K in simulation of silicic acid monomers.

at 1000 K are larger than at 1500 K, implying that while in general condensation is favoring larger cluster sizes as time goes on, reverse reactions are competing with cluster growth and the clusters may be less bonded to each other. This is also consistent with the analysis that at 1500 K denser clusters are formed with silicon that have a higher number of bridges as these clusters will be more difficult to break apart.

In order to determine the activation energy of condensation in this system, the concentration of silanol was used as a species in modeling reaction kinetics, similar to the procedures of Tan and Rankin.[11] As the hydroxysilanes condense, they will progressively form larger clusters, and the diffusion coefficient of these clusters decreases. The initial concentration rate data was fit to a second-order rate equation with respect to silanol concentration. Following the determination of the reaction rate coefficient, an Arrhenius plot was constructed in Figure 12.

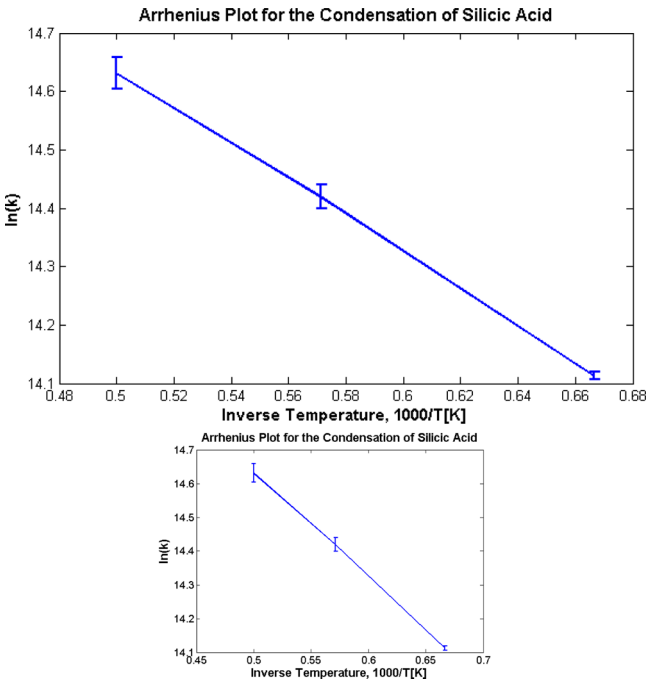

Figure 12. Arrhenius plot for condensation of pure silicic acid. Data corresponds to an activation energy of 6.2 ± 0.3 kcal/mol with pre-exponential factor of 1.08e7 ± 0.12e7 $(M\ sec)^{-1}$.

From the slope of this plot, it is determined that the condensation reaction of silicic acid is 6.2 ± 0.3 kcal/mol, with pre-exponential factor 1.08e7 ± 0.12e7M^{-1} sec^{-1}. This is within the expected range of activation energies typical to the hydrolysis and condensation of precursor solutions (5−15 kcal/mol.[14,15,20,21]). Other empirical molecular dynamics studies have reported activation energies from 13 to 15 kcal/mol for the polycondensation of silicic acid.[28,29] Even so, density functional theory investigations[20,79] have suggested that the activation energy of condensation decreases in an aqueous environment, due to hydrogen bond stabilization of the transition state. By extension, the condensation of silanols in pure silicic acid will also be catalyzed by neighboring hydrogen bonds. Also, considering that the force field developed in the present study was optimized against gas phase reaction energies, which are on average 20.0 kcal/mol higher, this result is reasonable.

Figure 13 shows the distribution of condensed Si−O−Si rings formed by the condensation of silicic acid at a temperature of 2000 K at 4 ns. The average number of silicons in condensed rings is 4.9 ± 1.4 atoms; this value is consistent with the results of other molecular dynamics studies, which find that five-member rings are the most common among silica gels formed by condensation of silicic acid.[28−30]

dx.doi.org/10.1021/jp504138r | J. Phys. Chem. B XXXX, XXX, XXX−XXX

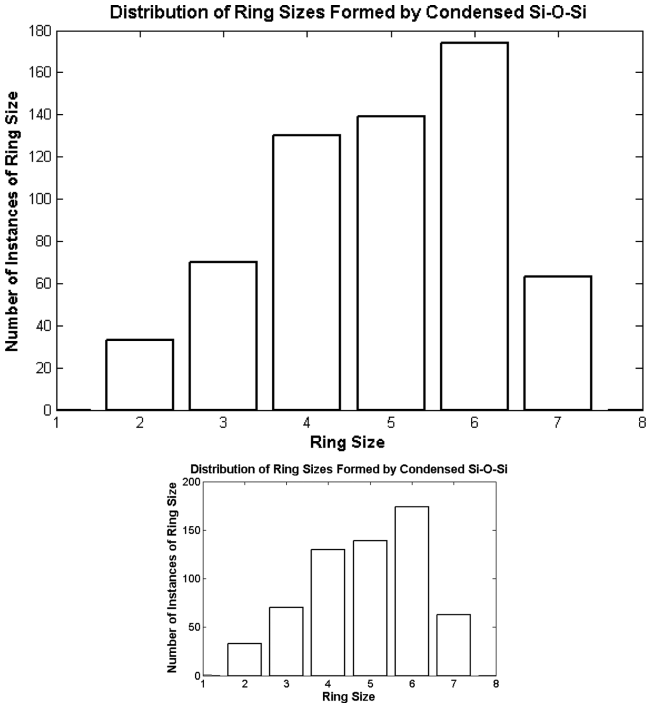

Figure 13. Condensed −Si−O−Si− ring distribution formed after simulation of silicic acid monomers for 4 ns at 2000 K. The average ring size is represented by 4.9 ± 1.4 silicon atoms.

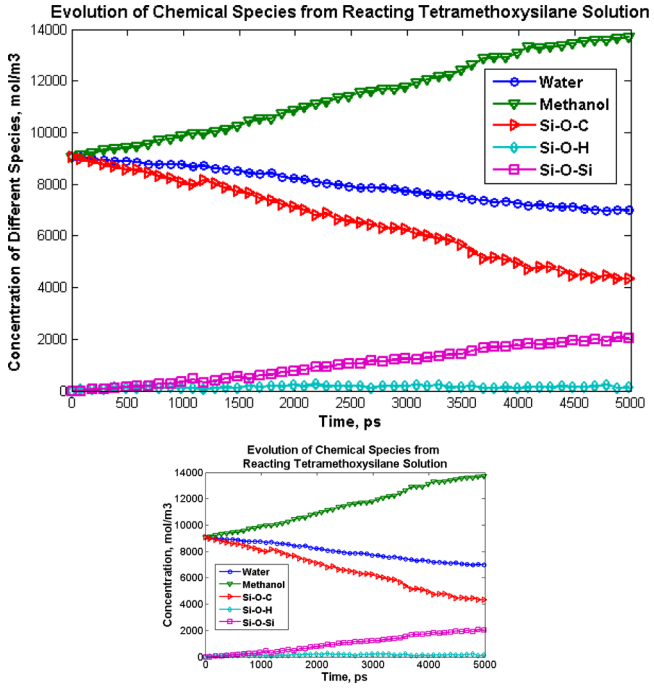

Figure 14. Temporal concentrations of chemical species from a reacting precursor solution containing a 1:4:4 mixture of tetramethoxysilane:methanol:water.

IIId. Case Study: Reacting Precursor Solution. Previous studies on the condensation of hydroxysilanes[25−30] have been beneficial in developing an understanding of gelation and the morphology of siloxanes. However, in all of these studies, only condensation reactions with pure silicic acid is modeled. In a typical precursor solution intended for generating sol−gels, normally a mixture of alkoxysilane, solvent, and water is used.[11] Considering the presence of these chemicals in the reacting solution adds complexity to modeling sol−gels. For instance, the effects solvation,[12,14] diffusion,[25] and the kinetics of both hydrolysis and condensation[11] must be considered. The model which has been developed in the present study is capable of simulating these systems. In this section, we aim to establish that the optimized force field can model both the hydrolysis and condensation reactions of chemicals in a precursor system. To this end, we have constructed a system consisting of a mixture of 100 tetramethoxysilane (TMOS), 400 methanol, and 400 water molecules added to a box with the dimensions $4.19 \times 4.19 \times 4.19$ nm^3. The initial positions of the molecules are randomly chosen by using Packmol[78] with the requirement that none of the atoms can be within 2 Å of each other. This system was simulated with a time step 0.25 fs in the canonical ensemble thermostatting the system to 2000 K. The temperature was maintained using the Nosé−Hoover thermostat[69,70] with the time constant of 25 fs. The system was simulated for a total of 5 ns. At this high temperature, we constrain nonreacting bonds as it has been previously shown[38] that simulation of PDMS at 2500 K can lead to the formation of decomposition products such as methane and hydrogen gas. Therefore, all oxygen−carbon bonds and carbon−hydrogen bonds are restrained to 1.43 and 1.10 Å, respectively, with a quadratic potential and energy coefficient 50.0 kcal/mol/Å^2.

Figure 14 shows the temporal evolution of chemical species from the precursor solution. The Si−O−C chemical groups from the TMOS are diminished over time by hydrolysis which generates methanol. Gradually, silanol generated during the hydrolysis step gives rise to condensed Si−O−Si bridges. The low concentration of silanol groups in the solution indicates that the rate-limiting step is the hydrolysis step at these conditions. This agrees with historical findings that at neutral conditions the rate of hydrolysis is at its slowest,[80] whereas the rate of condensation is faster in comparison.[81−83] The hydrolysis of precursor consumes a water molecule to generate an alcohol and a silanol, whereas condensation between two silanols produces water. The net effect between these two reactions is the consumption of water as condensation proceeds.

IV. CONCLUSIONS

A new parallel optimization tool has been developed in order to parametrize ReaxFF in a thorough and timely manner. This optimization procedure was applied to train a model for alkoxysilane gelation, but in practice, the procedure used here can be applied to parametrize any reacting system. The parallel implementation used here divides the parameter list among several nodes into smaller subsets. Using this approach results in much faster parametrizations of ReaxFF and also helps to prevent entrapment in local minima.

The time per iteration has been significantly reduced. In this study, a total of 136 iterations were used to optimize the parameter set. By using the older SPS algorithm, this optimization would have taken a total of 58 days to complete, assuming the 12 h of computing time per iteration determined in this study. By using the parallel optimization algorithm, only 3 days were needed. With a parallel parameter search, it is now more feasible to include thermodynamic information in the training set which previously would have required excessive computer time, such as liquid densities, diffusion coefficients,

dx.doi.org/10.1021/jp504138r | J. Phys. Chem. B XXXX, XXX, XXX−XXX

and free energies of mixing. To our knowledge, such properties have never been included in a parametrization of ReaxFF.

The optimized model is able to reproduce hydrolysis and condensation reaction data with reasonable accuracy, as well as match typical expectations of other properties, such as molecular geometry, bond dissociation energies, and atomic partial charges. The developed model is applied to model the polycondensation of tetrahydroxysilane at several temperatures. A gradual consumption of silanols is followed by condensed siloxane cluster growth, and finally densification. The activation energy of silane condensation is calculated to be within the expected range. Both hydrolysis and condensation of alkoxysilanes are seen in a simulation of a solution tetramethoxysilane, methanol, and water. In order for clusters obtained from the precursor solution to form a gel, additional simulation time will be needed. A model for simulating the dynamic condensation of alkoxysilane precursor in solution has been developed and will have useful applications in modeling surface attachment chemistry to bulk silica, as well as monitoring the kinetics and morphology of bulk gel formation.

■ ASSOCIATED CONTENT

Supporting Information

Additional figures comparing the performance of the parallel parameter search algorithm and SPS and relevant bond dissociation energy curves are provided. Additional figures from Case Study: Pure Silicic Acid Condensation are also included. This material is available free of charge via the Internet at http://pubs.acs.org.

■ AUTHOR INFORMATION

Corresponding Authors

*E-mail: jddeetz@ucdavis.edu.

*E-mail: rfaller@ucdavis.edu.

Notes

The authors declare no competing financial interest.

■ ACKNOWLEDGMENTS

This work benefitted from useful discussions with Prof. Adri van Duin.

■ REFERENCES

(1) Plueddemann, E. P. *Silane Coupling Agents*. Springer: New York, 1982.

(2) Booth, B. D.; Vilt, S. G.; Lewis, J. B.; Rivera, J. L.; Buehler, E. A.; McCabe, C.; Jennings, G. K. Tribological durability of silane monolayers on silicon. *Langmuir* **2011**, *27* (10), 5909−5917.

(3) Howarter, J. A.; Youngblood, J. P. Optimization of silica silanization by 3-aminopropyltriethoxysilane. *Langmuir* **2006**, *22* (26), 11142−11147.

(4) Vandenberg, E. T.; Bertilsson, L.; Liedberg, B.; Uvdal, K.; Erlandsson, R.; Elwing, H.; Lundström, I. Structure of 3-aminopropyl triethoxy silane on silicon oxide. *J. Colloid Interface Sci.* **1991**, *147* (1), 103−118.

(5) Hu, J.-M.; Liu, L.; Zhang, J.-Q.; Cao, C.-N. Electrodeposition of silane films on aluminum alloys for corrosion protection. *Prog. Org. Coat.* **2007**, *58* (4), 265−271.

(6) Li, Y.-S.; Ba, A. Spectroscopic studies of triethoxysilane sol−gel and coating process. *Spectrochim. Acta, Part A* **2008**, *70* (5), 1013−1019.

(7) Zeno, W. F.; Longo, M. L.; Risbud, S. H.; Coleman, M. A. Investigation of Nanolipoprotein Particles Entrapped Within Nanoporous Silica: A Novel Platform for Immobilization of Integral Membrane Proteins. *Biophys. J.* **2014**, *106* (2), 421a.

(8) Schmidt, H.; Scholze, H.; Kaiser, A. Principles of Hydrolysis and Condensation Reaction of Alkoxysilanes. *J. Non-Cryst. Solids* **1984**, *63* (1), 1−11.

(9) Loy, D. A.; Baugher, B. M.; Baugher, C. R.; Schneider, D. A.; Rahimian, K. Substituent Effects on the Sol-Gel Chemistry of Organotrialkoxysilanes. *Chem. Mater.* **2000**, *12* (12), 3624−3632.

(10) Vainrub, A.; Devreux, F.; Boilot, J.; Chaput, F.; Sarkar, M. Sol-Gel Polymerization in Alkoxysilanes: ^{29}Si NMR Study and Simulation of Chemical Kinetics. *Mater. Sci. Eng., B* **1996**, *37* (1), 197−200.

(11) Tan, B.; Rankin, S. E. Study of the Effects of Progressive Changes in Alkoxysilane Structure on Sol-Gel Reactivity. *J. Phys. Chem. B* **2006**, *110* (45), 22353−22364.

(12) Bernards, T.; Van Bommel, M.; Boonstra, A. Hydrolysis-Condensation Processes of the Tetra-Alkoxysilanes TPOS, TEOS and TMOS in Some Alcoholic Solvents. *J. Non-Cryst. Solids* **1991**, *134* (1), 1−13.

(13) Matejka, L.; Dukh, O.; Hlavatá, D.; Meissner, B.; Brus, J. Cyclization and Self-Organization in Polymerization of Trialkoxysilanes. *Macromolecules* **2001**, *34* (20), 6904−6914.

(14) Jiang, H.; Zheng, Z.; Wang, X. Kinetic Study of Methyltriethoxysilane (MTES) Hydrolysis by FTIR Spectroscopy under Different Temperatures and Solvents. *Vib. Spectrosc.* **2008**, *46* (1), 1−7.

(15) Colby, M. W.; Osaka, A.; Mackenzie, J. D. Temperature Dependence of the Gelation of Silicon Alkoxides. *J. Non-Cryst. Solids* **1988**, *99* (1), 129−139.

(16) Pereira, J.; Catlow, C.; Price, G. Molecular Dynamics Simulation of Methanolic and Ethanolic Silica-Based Sol-Gel Solutions at Ambient Temperature and Pressure. *J. Phys. Chem. A* **2002**, *106* (1), 130−148.

(17) Pereira, J.; Catlow, C.; Price, G. Molecular Dynamics Simulation of Liquid H2O, MeOH, EtOH, Si(OMe)4, and Si(OEt)4, as a Function of Temperature and Pressure. *J. Phys. Chem. A* **2001**, *105* (10), 1909−1925.

(18) Kornherr, A.; Hansal, S.; Hansal, W. E.; Besenhard, J. O.; Kronberger, H.; Nauer, G. E.; Zifferer, G. Molecular Dynamics Simulations of the Adsorption of Industrial Relevant Silane Molecules at a Zinc Oxide Surface. *J. Chem. Phys.* **2003**, *119*, 9719−9728.

(19) Kornherr, A.; Nauer, G. E.; Sokol, A. A.; French, S. A.; Catlow, C. R. A.; Zifferer, G. Adsorption of Organosilanes at a Zn-Terminated ZnO (0001) Surface: Molecular Dynamics Study. *Langmuir* **2006**, *22* (19), 8036−8042.

(20) Okumoto, S.; Fujita, N.; Yamabe, S. Theoretical Study of Hydrolysis and Condensation of Silicon Alkoxides. *J. Phys. Chem. A* **1998**, *102* (22), 3991−3998.

(21) Elanany, M.; Selvam, P.; Yokosuka, T.; Takami, S.; Kubo, M.; Imamura, A.; Miyamoto, A. A Quantum Molecular Dynamics Simulation Study of the Initial Hydrolysis Step in Sol-Gel Process. *J. Phys. Chem. B* **2003**, *107* (7), 1518−1524.

(22) Zipoli, F.; Donadio, D.; Bernasconi, M. Simulation of the Grafting of Organosilanes at the Surface of Dry Amorphous Silica. *J. Phys.: Condens. Matter* **2008**, *20* (22), 224011.

(23) Pereira, J.; Catlow, C.; Price, G. Ab Initio Studies of Silica-Based Clusters. Part II. Structures and Energies of Complex Clusters. *J. Phys. Chem. A* **1999**, *103* (17), 3268−3284.

(24) Pereira, J.; Catlow, C.; Price, G. Ab Initio Studies of Silica-Based Clusters. Part I. Energies and Conformations of Simple Clusters. *J. Phys. Chem. A* **1999**, *103* (17), 3252−3267.

(25) Bhattacharya, S.; Kieffer, J. Molecular Dynamics Simulation Study of Growth Regimes during Polycondensation of Silicic Acid: From Silica Nanoparticles to Porous Gels. *J. Phys. Chem. C* **2008**, *112* (6), 1764−1771.

(26) Bhattacharya, S.; Kieffer, J. Fractal Dimensions of Silica Gels Generated Using Reactive Molecular Dynamics Simulations. *J. Chem. Phys.* **2005**, *122*, 094715.

(27) Feuston, B.; Garofalini, S. Oligomerization in Silica Sols. *J. Phys. Chem.* **1990**, *94* (13), 5351−5356.

(28) Garofalini, S. H.; Martin, G. Molecular Simulations of the Polymerization of Silicic Acid Molecules and Network Formation. *J. Phys. Chem.* **1994**, *98* (4), 1311−1316.

(29) Rao, N. Z.; Gelb, L. D. Molecular Dynamics Simulations of the Polymerization of Aqueous Silicic Acid and Analysis of the Effects of Concentration on Silica Polymorph Distributions, Growth Mechanisms, And Reaction Kinetics. *J. Phys. Chem. B* **2004**, *108* (33), 12418−12428.
(30) Yamahara, K.; Okazaki, K. Molecular Dynamics Simulation of the Structural Development in Sol−gel Process for Silica Systems. *Fluid Phase Equilib.* **1998**, *144* (1), 449−459.
(31) Gygi, F.; Yates, R. K.; Lorenz, J.; Draeger, E. W.; Franchetti, F.; Ueberhuber, C. W.; Supinski, B. R. d.; Kral, S.; Gunnels, J. A.; Sexton, J. C. In *Large-Scale First-Principles Molecular Dynamics Simulations on the Bluegene/L Platform Using the Qbox Code*, Proceedings of the 2005 ACM/IEEE Conference on Supercomputing, IEEE Computer Society: Washington, D.C., 2005; p 24.
(32) Chenoweth, K.; van Duin, A. C. T.; Goddard, W. A. ReaxFF Reactive Force Field for Molecular Dynamics Simulations of Hydrocarbon Oxidation. *J. Phys. Chem. A* **2008**, *112* (5), 1040−1053.
(33) van Duin, A. C. T.; Dasgupta, S.; Lorant, F.; Goddard, W. A. ReaxFF: A reactive force field for hydrocarbons. *J. Phys. Chem. A* **2001**, *105* (41), 9396−9409.
(34) Strachan, A.; Kober, E. M.; van Duin, A. C.; Oxgaard, J.; Goddard, W. A., III Thermal Decomposition of RDX from Reactive Molecular Dynamics. *J. Chem. Phys.* **2005**, *122*, 054502.
(35) Van Duin, A. C.; Strachan, A.; Stewman, S.; Zhang, Q.; Xu, X.; Goddard, W. A. ReaxFFSiO Reactive Force Field for Silicon and Silicon Oxide Systems. *J. Phys. Chem. A* **2003**, *107* (19), 3803−3811.
(36) Fogarty, J. C.; Aktulga, H. M.; Grama, A. Y.; Van Duin, A. C.; Pandit, S. A. A Reactive Molecular Dynamics Simulation of the Silica-Water Interface. *J. Chem. Phys.* **2010**, *132*, 174704.
(37) Newsome, D. A.; Sengupta, D.; Foroutan, H.; Russo, M. F.; van Duin, A. C. Oxidation of Silicon Carbide by O2 and H2O: A ReaxFF Reactive Molecular Dynamics Study, Part I. *J. Phys. Chem. C* **2012**, *116* (30), 16111−16121.
(38) Chenoweth, K.; Cheung, S.; van Duin, A. C. T.; Goddard, W. A.; Kober, E. M. Simulations on the Thermal Decomposition of a Poly(dimethylsiloxane) Polymer Using the ReaxFF Reactive Force Field. *J. Am. Chem. Soc.* **2005**, *127* (19), 7192−7202.
(39) van Duin, A. C. T.; Baas, J. M. A.; van de Graaf, B. Delft Molecular Mechanics: A New Approach to Hydrocarbon Force Fields. Inclusion of a Geometry-Dependent Charge Calculation. *J. Chem. Soc., Faraday Trans.* **1994**, *90* (19), 2881−2895.
(40) Pahari, P.; Chaturvedi, S. Determination of best-fit potential parameters for a reactive force field using a genetic algorithm. *J. Mol. Model.* **2012**, *18* (3), 1049−1061.
(41) Larsson, H. R.; Duin, A. C.; Hartke, B. Global optimization of parameters in the reactive force field ReaxFF for SiOH. *J. Comput. Chem.* **2013**, *34* (25), 2178−2189.
(42) Larsson, H. R.; Hartke, B. Fitting Reactive Force Fields Using Genetic Algorithms. *Computer Methods in Materials Science* **2013**, *13*, 120−126.
(43) Jaramillo-Botero, A.; Naserifar, S.; Goddard, W. A., III General Multiobjective Force Field Optimization Framework, with Application to Reactive Force Fields for Silicon Carbide. *J. Chem. Theory Comput.* **2014**, *10* (4), 1426−1439.
(44) Iype, E.; Hütter, M.; Jansen, A.; Nedea, S. V.; Rindt, C. Parameterization of a Reactive Force Field Using a Monte Carlo Algorithm. *J. Comput. Chem.* **2013**, *34* (13), 1143−1154.
(45) Pauling, L. *The Nature of the Chemical Bond and the Structure of Molecules and Crystals: An Introduction to Modern Structural Chemistry*; Cornell University Press: Ithica, NY, 1960; Vol. *18*.
(46) Anderson, R.; Mayr, E. *Parallelism and Greedy Algorithms*; Department of Computer Science: Stanford University, 1984.
(47) Mortier, W. J.; Ghosh, S. K.; Shankar, S. Electronegativity-Equalization Method for the Calculation of Atomic Charges in Molecules. *J. Am. Chem. Soc.* **1986**, *108* (15), 4315−4320.
(48) Plimpton, S. Fast Parallel Algorithms for Short-Range Molecular Dynamics. *J. Comput. Phys.* **1995**, *117* (1), 1−19.
(49) Aktulga, H. M.; Fogarty, J. C.; Pandit, S. A.; Grama, A. Y. Parallel Reactive Molecular Dynamics: Numerical Methods and Algorithmic Techniques. *Parallel Computing* **2012**, *38* (4), 245−259.
(50) Eaton, J. W.; Bateman, D.; Hauberg, S. *GNU Octave Version 3.0. 1 Manual: A High-Level Interactive Language for Numerical Computations*. SoHo Books: New York, 2007.
(51) Frisch, M.; Trucks, G.; Schlegel, H.; Scuseria, G.; Robb, M.; Cheeseman, J.; Montgomery, J.; Vreven, T.; Kudin, K.; Burant, J. *Gaussian 03*, revision C. 02, 2008.
(52) Becke, A. D. Density-functional thermochemistry. III. The role of exact exchange. *J. Chem. Phys.* **1993**, *98* (7), 5648−5652.
(53) Lee, C.; Yang, W.; Parr, R. G. Development of the Colle-Salvetti Correlation-Energy Formula into a Functional of the Electron Density. *Phys. Rev. B* **1988**, *37* (2), 785.
(54) Krishnan, R.; Binkley, J. S.; Seeger, R.; Pople, J. A. Self-Consistent Molecular Orbital Methods. XX. A Basis Set for Correlated Wave Functions. *J. Chem. Phys.* **2008**, *72* (1), 650−654.
(55) McLean, A.; Chandler, G. Contracted Gaussian Basis Sets for Molecular Calculations. I. Second Row Atoms, Z = 11−18. *J. Chem. Phys.* **2008**, *72* (10), 5639−5648.
(56) Schlegel, H. B. Optimization of Equilibrium Geometries and Transition Structures. *J. Comput. Chem.* **1982**, *3* (2), 214−218.
(57) Gonzalez, C.; Schlegel, H. B. Reaction Path Following in Mass-Weighted Internal Coordinates. *J. Phys. Chem.* **1990**, *94* (14), 5523−5527.
(58) Gonzalez, C.; Schlegel, H. B. An Improved Algorithm for Reaction Path Following. *J. Chem. Phys.* **1989**, *90*, 2154.
(59) Møller, C.; Plesset, M. S. Note on an Approximation Treatment for Many-Electron Systems. *Phys. Rev.* **1934**, *46* (7), 618−622.
(60) Breneman, C. M.; Wiberg, K. B. Determining Atom-Centered Monopoles from Molecular Electrostatic Potentials. The Need for High Sampling Density in Formamide Conformational Analysis. *J. Comput. Chem.* **1990**, *11* (3), 361−373.
(61) Pluth, J.; Smith, J.; Faber, J., Jr. Crystal Structure of Low Cristobalite at 10, 293, and 473 K: Variation of Framework Geometry with Temperature. *J. Appl. Phys.* **1985**, *57* (4), 1045−1049.
(62) Jonsson, P. Hydrogen Bond Studies. CXIII. The Crystal Structure of Ethanol at 87 K. *Acta Crystallogr., Sect. B: Struct. Crystallogr. Cryst. Chem.* **1976**, *32* (1), 232−235.
(63) Bernal, J. D.; Fowler, R. H. A Theory of Water and Ionic Solution, with Particular Reference to Hydrogen and Hydroxyl Ions. *J. Chem. Phys.* **1933**, *1* (8), 515−548.
(64) Sun, H. COMPASS: An Ab Initio Force-Field Optimized for Condensed-Phase Applications Overview with Details on Alkane and Benzene Compounds. *J. Phys. Chem. B* **1998**, *102* (38), 7338−7364.
(65) Brooks, B. R.; Bruccoleri, R. E.; Olafson, B. D.; States, D. J.; Swaminathan, S.; Karplus, M. CHARMM: A Program for Macromolecular Energy, Minimization, And Dynamics Calculations. *J. Comput. Chem.* **1983**, *4* (2), 187−217.
(66) Liu, L.; Liu, Y.; Zybin, S. V.; Sun, H.; Goddard, W. A., III ReaxFF-lg: Correction of the ReaxFF Reactive Force Field for London Dispersion, With Applications to the Equations of State for Energetic Materials. *J. Phys. Chem. A* **2011**, *115* (40), 11016−11022.
(67) Parrinello, M.; Rahman, A. Polymorphic Transitions in Single Crystals: A New Molecular Dynamics Method. *J. Appl. Phys.* **1981**, *52* (12), 7182−7190.
(68) Shinoda, W.; Shiga, M.; Mikami, M. Rapid Estimation of Elastic Constants by Molecular Dynamics Simulation under Constant Stress. *Phys. Rev. B* **2004**, *69* (13), 134103.
(69) Nosé, S. A Unified Formulation of the Constant Temperature Molecular Dynamics Methods. *J. Chem. Phys.* **1984**, *81* (1), 511−519.
(70) Hoover, W. G. Canonical Dynamics: Equilibrium Phase-Space Distributions. *Phys. Rev. A* **1985**, *31* (3), 1695.
(71) Mitzel, N. W.; Blake, A. J.; Rankin, D. W. *β*-Donor Bonds in SiON Units: An Inherent Structure-Determining Property Leading to (4+ 4)-Coordination in Tetrakis-(*N*,*N*-dimethylhydroxylamido) Silane. *J. Am. Chem. Soc.* **1997**, *119* (18), 4143−4148.

(72) Tornroos, K. W. Octahydridosilasesquioxane Determined by Neutron Diffraction. *Acta Crystallogr., Sect. C: Cryst. Struct. Commun.* **1994**, *50* (11), 1646−1648.
(73) Kirchner, M. T.; Das, D.; Boese, R. Cocrystallization with Acetylene: Molecular Complex with Methanol. *Cryst. Growth Des.* **2008**, *8* (3), 763−765.
(74) Bream, R.; Watkin, D. Trans-1,4-Dimethylcyclohexane. *Acta Crystallogr., Sect. E: Struct. Rep. Online* **2006**, *62* (2), o414−o415.
(75) Lide, D. R. *CRC Handbook of Chemistry and Physics*. CRC Press: Boca Raton, FL, 2004.
(76) Methyltrimethoxysilane Methyltrimethoxysilane. http://www.chemspider.com/Chemical-Structure.13803.html (accessed March 10, 2013).
(77) Trimethoxysilane Methyltrimethoxysilane. http://www.chemspider.com/Chemical-Structure.13803.html (accessed Feb 3, 2014).
(78) Martínez, L.; Andrade, R.; Birgin, E. G.; Martínez, J. M. Packmol: A package for building initial configurations for molecular dynamics simulations. *J. Comput. Chem.* **2009**, *30* (13), 2157−2164.
(79) Burggraf, L. W.; Davis, L. P.; Gordon, M. S. *Ultrastructure Processing of Advanced Materials*; Wiley and Sons: Hoboken, NJ, 1992, p 47.
(80) Pohl, E.; Osterholtz, F. Kinetics and Mechanism of Aqueous Hydrolysis and Condensation of Alkyltrialkoxysilanes. In *Molecular Characterization of Composite Interfaces*; Springer: New York, 1985; pp 157−170.
(81) Brinker, C. Hydrolysis and Condensation of Silicates: Effects on Structure. *J. Non-Cryst. Solids* **1988**, *100* (1), 31−50.
(82) Brinker, C. J.; Scherer, G. W. *Sol-Gel Science: The Physics and Chemistry of Sol-Gel Processing*; Gulf Professional Publishing: Houston, TX, 1990.
(83) Pope, E.; Mackenzie, J. Sol-Gel Processing of Silica: II. The Role of the Catalyst. *J. Non-Cryst. Solids* **1986**, *87* (1), 185−198.